

Silicon microspectrometer chip based on nanostructured fishnet photodetectors with tailored responsivities and machine learning: supplementary material

JASPER J. CADUSCH,^{1,3} JIAJUN MENG,¹ BENJAMIN CRAIG,² AND KENNETH B. CROZIER^{1,2,4}

¹ Department of Electrical and Electronic Engineering, The University of Melbourne, Victoria 3010, Australia

² School of Physics, The University of Melbourne, Victoria 3010, Australia

³ caduschj@unimelb.edu.au

⁴ kenneth.crozier@unimelb.edu.au

Published 10 September 2019

This document provides supplementary information to "Silicon microspectrometer chip based on nanostructured fishnet photodetectors with tailored responsivities and machine learning,"

<https://doi.org/10.1364/optica.6.001171>.

Waveguide Array Modes:

Our fishnet structures consist of two arrays of vertical dielectric slab waveguides (orthogonal to one another). We thus expect that the optical response of our fishnet structures can be understood by considering them to be high contrast gratings (HCGs). The work of Chang-Hasnain et al provides explicit details on the physics of such structures[1], including a derivation of dispersion relation used in the work presented here. The primary difference between a stand-alone vertical slab waveguide and a near-wavelength waveguide array (WGA) is that for the stand-alone case near the cut-off wavelength of a mode, energy from that mode is mostly directed out of the waveguide sidewalls that is, the fields close to cut-off become spread out, well beyond the core of the waveguide. For the WGA case near cut-off the fields from each waveguide mode extend well beyond the sidewalls of one waveguide and into the neighboring waveguide through its sidewalls and so on. So near a mode cut-off wavelength the guided light interacts with multiple neighboring waveguides in the array. Now, when operating the waveguide where the materials optical properties lead to strong absorption of light, such as visible light in silicon, this process can lead to very large fractional absorption coefficients. For example, Figure S1(a) shows FEM simulations for a 400 nm period WGA illuminated with normally incident TE polarized light. The red curves show the cut-off wavelengths for the TE₂, TE₄ and TE₆ modes, as given by HCG theory. It can be seen that similar to the TM mode behavior, the fractional absorption peaks near the calculated mode cut-off wavelengths. Figures S1(b)&(c) show the effect of array period on the mode cut-off wavelengths. Figure S1(b) shows the TM₂ mode cut-off as a function of waveguide thickness for six different array periods. It is clear that as period increases, the TM₂ cut-off wavelengths red-shift. This is a useful feature, since it is much easier to control the array period during fabrication than controlling the waveguide widths that result after etching. Figure S1(c) shows the cut-off wavelengths for several (even) TM and TE modes as a

function of period, Λ , for a set of 135 nm wide waveguides. Here we see that the modes are mostly non-degenerate except at certain values of Λ . We also see that as we move to higher order modes, the mode spacing reduces. This leads to wider absorption bands at these wavelengths.

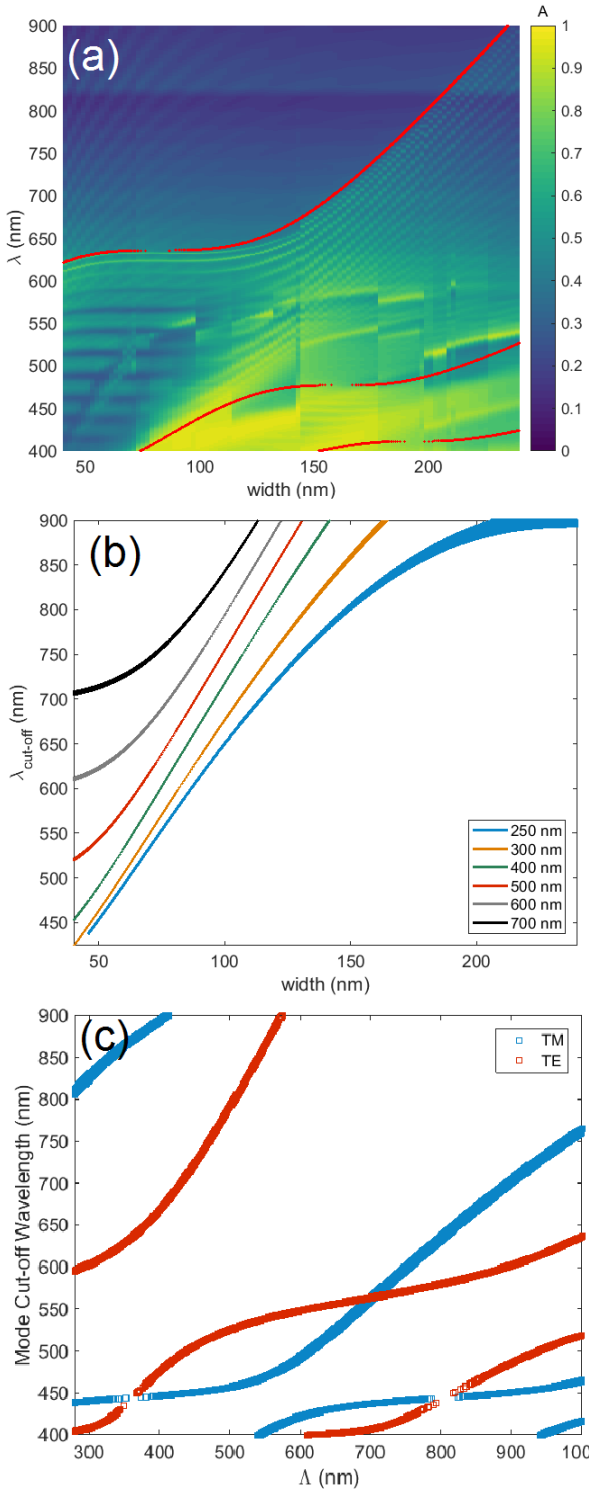


Figure S1: (a) FEM absorption calculations for a 400 nm period WGA illuminated with TE polarized light, with theoretical mode cut-off wavelengths shown in red. (b) TE₂ mode cut-off wavelengths for a set of waveguides as a function of waveguide widths with varied array periods from 250 nm to 700 nm. (c) Mode cut-off wavelengths for 135 nm wide waveguides as a function of array period. TM modes: blue curves. TE modes: red curves.

Supervised Machine Learning Based Spectral Reconstruction:

Consider N detectors illuminated with an unknown spectrum $S(\lambda)$. The responsivities of the detectors are known and denoted $R_i(\lambda)$. The generated photocurrent for the i^{th} detector is

$$P_i = \int R_i(\lambda)S(\lambda)d\lambda, \quad i \in \{1,2, \dots, N\} \quad (\text{S1})$$

In our spectral reconstruction algorithm, we wish to solve equation S1 for $S(\lambda)$. Since our responsivities are measured in a discrete fashion (5 nm steps in our case) we must discretize S1 into M wavelengths. Doing so yields

$$P = RS \quad (\text{S2})$$

Where P and S are $N \times 1$ and $M \times 1$ vectors, respectively, and R is an $N \times M$ matrix with element ij corresponding to the i^{th} detector and j^{th} wavelength, λ_j .

Clearly to solve for S by inverting R in this case is only possible when $N = M$ and other methods will fail when $N < M$, since there are more unknown values than simultaneous equations to solve. However, we can apply a transformation matrix, T , to R and S to reduce the number of unknowns in the system. Here following Kurokawa *et al.*, we set T to be comprised of a set of Gaussian vectors centered on λ_j such that $R_r = RT$ and $S = TS_r$, where R_r and S_r are the reduced responsivity matrix and unknown spectrum vector, respectively. Clearly T must be a $M \times N$ matrix so that R_r is an $N \times N$ matrix and S_r is a $N \times 1$ vector. Equation (S2) then becomes

$$P = R_r S_r \quad (\text{S3})$$

which could be solved for S_r and (mapped back to S , the unknown spectrum, using $S = TS_r$), with the method of least squares to find $\min_{S_r} \|R_r S_r - P\|_2^2$ or perhaps direct inversion if

$\det(R_r) \neq 0$. In the work presented here we use two sets of Gaussian basis vectors to form T , with one set used to represent the fishnet responsivities and the other set the mesas. We center the twenty fishnet Gaussian vectors at wavelengths from 400 nm to 550 nm, with 5 nm steps and assign an FWHM of 85 nm. For the 20 mesa vectors, we span a range of 550 nm to 800 nm with 5 nm steps and a width of 550 nm. These values roughly correspond to the measured responsivity curves but were found via optimization.

Since both responsivities and photocurrent measurements will contain random observation noise, which for such an ill-conditioned system will make using the method of least squares fruitless, we arrive at the need for Tikhonov regularization (also known as weight decay or ridge regression). We find the regularization parameter using the L-curve method, and restrict the values of S_r to be non-negative since negative spectral values are unphysical[2]. Figure S2 shows the measured and reconstructed spectrum from a white light LED lamp using this regularization technique. Our method is able to identify the correct locations of both peaks as well as their relative amplitudes, but the linewidths of each feature are incorrect.

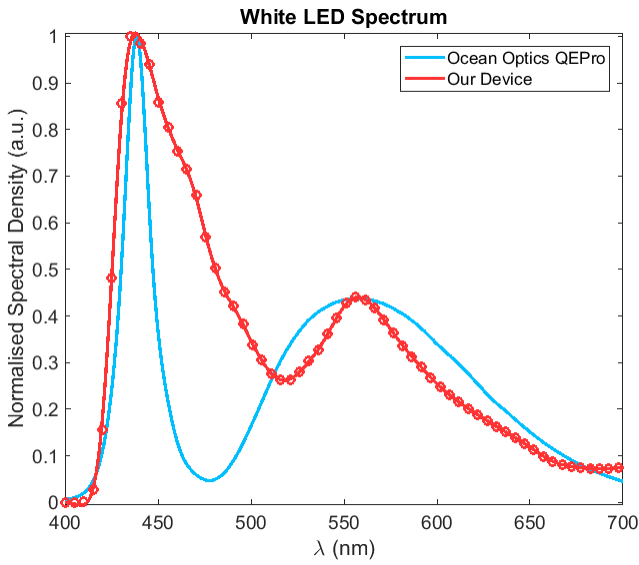


Figure S2: Measured and Tikhonov regularized reconstructed spectrum of the white LED lamp, prior to simulated annealing.

To improve the reconstruction further, we implemented a simulated annealing step with the regularized output as an initial guess. We used the algorithm of Redding et al to achieve improved reconstructions[3]. Here we use a linear cooling schedule with an initial temperature of 10,500, with a random multiplier between 0.4 and 1.3 and stop the algorithm either when the system energy, that is the difference between the measured photocurrents and calculated photocurrents using equation (S2) with our reconstructed spectrum, drops below 0.0005 or after 1200 iterations, when the temperature reaches 0. To improve the reliability and reproducibility of the simulated annealing algorithm used by Redding et al, we run our algorithm 1000 times and take the reconstructed spectrum with the final system energy closest to the median final system energy of the 1000 trials.

Fishnet Number: Since our microspectrometer consists of 20 fishnet pixels with varied waveguide widths and array periods we give each pixel a “fishnet number” to identify it. Table S1 gives a summary of the width, period and peak responsivity wavelength for each fishnet number.

Fishnet Number	Waveguide Width (nm)	Array Period (nm)	Wavelength (nm)
1	95	325	400
2	90	425	405
3	105	350	410
4	105	325	410
5	160	500	420
6	160	535	420
7	105	425	420
8	170	375	430
9	105	375	455
10	140	425	460
11	150	550	460
12	110	400	490
13	130	400	485
14	110	350	480
15	110	300	495
16	120	425	520
17	120	400	510
18	110	325	530
19	130	425	505
20	160	375	465

Table S1. Width, period and responsivity peak wavelength for each microspectrometer pixel, identified by fishnet number.

Photodiode Power Dependence and Linearity:

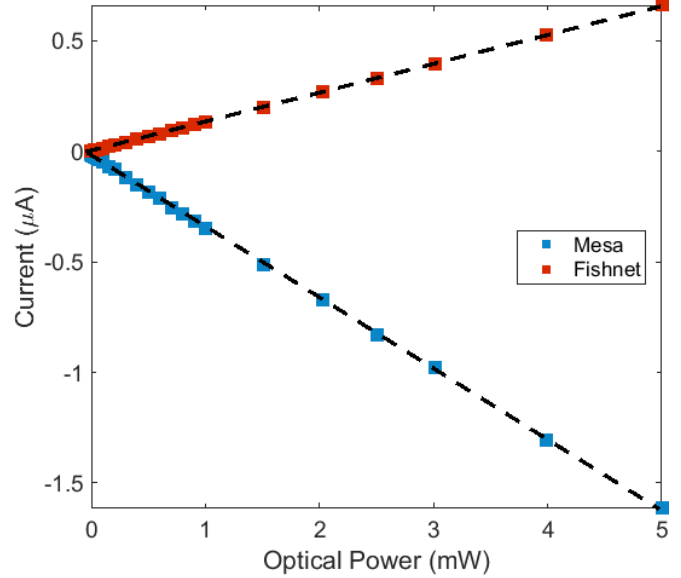


Figure S3: Measured photocurrent generated in fishnet (red squares) and mesa (blue squares) number 8 when illuminated with the LED lamp, with varied optical power. The dashed lines are to guide the eye.

To verify the current output from both mesa and fishnet detectors vary linearly with optical power we measure the photoresponse for fishnet pixel number 8. The optical power was increased from 1 μ W to 5 mW and the photocurrent measured for -1 V (mesa) and +1 V (fishnet) bias voltage. Figure S3 shows that for this range of powers both mesa and fishnet detectors can be expected to behave linearly.

References

1. C. J. Chang-Hasnain, and W. Yang, "High-contrast gratings for integrated optoelectronics," *Advances in Optics and Photonics* **4**, 379-440 (2012).
2. U. Kurokawa, B. I. Choi, and C.-C. Chang, "Filter-based miniature spectrometers: spectrum reconstruction using adaptive regularization," *IEEE Sensors Journal* **11**, 1556-1563 (2011).
3. B. Redding, S. M. Popoff, and H. Cao, "All-fiber spectrometer based on speckle pattern reconstruction," *Optics Express* **21**, 6584-6600 (2013).